#### Uncovering novel mutational signatures by *de novo* extraction with 1

#### **SigProfilerExtractor** 2

- S M Ashiqul Islam<sup>1,2,3</sup>, Yang Wu<sup>4</sup>, Marcos Díaz-Gay<sup>1,2,3</sup>, Erik N Bergstrom<sup>1,2,3</sup>, Yudou He<sup>1,2,3</sup>, 3
- Mark Barnes<sup>1,2,3</sup>, Mike Vella<sup>5</sup>, Jingwei Wang<sup>6</sup>, Jon W Teague<sup>6</sup>, Peter Clapham<sup>6</sup>, Sarah Moody<sup>6</sup>, 4
- Sergey Senkin<sup>7</sup>, Yun Rose Li<sup>8</sup>, Laura Riva<sup>6</sup>, Tongwu Zhang<sup>9</sup>, Andreas J Gruber<sup>10,11</sup>, Raviteja 5
- Vangara<sup>12</sup>, Christopher D Steele<sup>13</sup>, Burçak Otlu<sup>1,2,3</sup>, Azhar Khandekar<sup>1,2,3</sup>, Ammal Abbasi<sup>1,2,3</sup>, 6
- 7 Laura Humphreys<sup>6</sup>, Natalia Syulyukina<sup>2</sup>, Samuel W Brady<sup>14</sup>, Boian S Alexandrov<sup>11</sup>, Nischalan
- 8 Pillay<sup>13,15</sup>, Jinghui Zhang<sup>14</sup>, David J Adams<sup>6</sup>, Iñigo Marticorena<sup>6</sup>, David C Wedge<sup>10,11</sup>, Maria
- 9 Teresa Landi<sup>9</sup>, Paul Brennan<sup>7</sup>, Michael R Stratton<sup>6</sup>, Steven G Rozen<sup>4</sup>, and Ludmil B
- 10 Alexandrov<sup>1,2,3\*</sup>
- 11
- 12

#### 13 Affiliations

- 14 <sup>1</sup>Department of Cellular and Molecular Medicine, UC San Diego, La Jolla, CA, 92093, USA
- 15 <sup>2</sup>Department of Bioengineering, UC San Diego, La Jolla, CA, 92093, USA
- 16 <sup>3</sup>Moores Cancer Center, UC San Diego, La Jolla, CA, 92037, USA
- 17 <sup>4</sup>Centre for Computational Biology and Programme in Cancer & Stem Cell Biology, Duke NUS
- 18 Medical School, 169857, Singapore
- 19 <sup>5</sup>NVIDIA Corporation, 2788 San Tomas Expressway, Santa Clara, CA, 95051, USA
- 20 <sup>6</sup>Cancer, Ageing and Somatic Mutation, Wellcome Sanger Institute, Wellcome Genome Campus,
- 21 Cambridge, CB10 1SA, UK
- 22 <sup>7</sup>Genetic Epidemiology Group, International Agency for Research on Cancer, 69372 Lyon CEDEX
- 23 08. France
- 24 <sup>8</sup>Helen Diller Family Comprehensive Cancer Center, San Francisco, CA, 94158, USA
- 25 <sup>9</sup>Division of Cancer Epidemiology and Genetics, National Cancer Institute, Bethesda, MD, 20892, 26 USA
- 27 <sup>10</sup>Big Data Institute, Nuffield Department of Medicine, University of Oxford, OX5 7LF, 28 UK
- 29 <sup>11</sup>Manchester Cancer Research Centre, The University of Manchester, Manchester, M20 4GJ, UK
- 30 <sup>12</sup>Theoretical Division, Los Alamos National Laboratory, Los Alamos, NM, 87545, USA
- 31 <sup>13</sup>Research Department of Pathology, Cancer Institute, University College London, London, WC1E 32 6BT. UK
- 33 <sup>14</sup>Department of Computational Biology, St. Jude Children's Research Hospital, Memphis, 38105,
- 34 Tennessee, USA
- 35 <sup>15</sup>Department of Cellular and Molecular Pathology, Royal National Orthopaedic Hospital NHS
- 36 Trust, Stanmore, Middlesex, HA7 4LP, UK
- 37
- 38 \*Correspondence should be addressed to L2alexandrov@health.ucsd.edu.
- 39

# 40 ABSTRACT

41 Mutational signature analysis is commonly performed in genomic studies surveying cancer and 42 normal somatic tissues. Here we present SigProfilerExtractor, an automated tool for accurate de 43 novo extraction of mutational signatures for all types of somatic mutations. Benchmarking with a 44 total of 33 distinct scenarios encompassing 1,106 simulated signatures operative in more than 45 200,000 synthetic genomes demonstrates that SigProfilerExtractor outperforms ten other tools 46 across all datasets with and without noise. For simulations with 5% noise, reflecting high-quality 47 genomic datasets, SigProfilerExtractor outperforms other approaches by elucidating between 48 20% and 50% more true positive signatures while yielding more than 5-fold less false positive 49 signatures. Applying SigProfilerExtractor to 2,778 whole-genome sequenced cancers reveals 50 three previously missed mutational signatures. Two of the signatures are confirmed in 51 independent cohorts with one of these signatures associating with tobacco smoking. In summary, 52 this report provides a reference tool for analysis of mutational signatures, a comprehensive 53 benchmarking of bioinformatics tools for extracting mutational signatures, and several novel 54 mutational signatures including a signature putatively attributed to direct tobacco smoking 55 mutagenesis in bladder cancer and in normal bladder epithelium.

## 57 INTRODUCTION

*De novo* extraction of mutational signatures<sup>1</sup> is an unsupervised machine learning approach 58 59 where a matrix, M, which corresponds to the somatic mutations in a set of cancer genomes under 60 a mutational classification<sup>2</sup>, is approximated by the product of two low-rank matrices, S and A. 61 The matrix **S** reflects the set of mutational signatures while the matrix **A** encompasses the 62 activities of the signatures; an activity corresponds to the number of mutations contributed by a 63 signature in a sample. Algorithmically, *de novo* extraction of mutational signatures has relied on nonnegative matrix factorization  $(NMF)^3$  or on approaches mathematically analogous to  $NMF^{4-6}$ . 64 65 The main advantage of NMF over other factorization approaches is its ability to yield 66 nonnegative factors that are part of the original data, thus, allowing interpretation of the 67 identified nonnegative factors<sup>3</sup>. Biologically, mutational signatures extracted from cancer 68 genomes have been attributed to exposures to environmental carcinogens, failure of DNA repair 69 pathways, infidelity/deficiency of replicating polymerases, iatrogenic events, and others<sup>7-14</sup>. 70 71 Since we introduced the mathematical concept of mutational signatures<sup>1</sup>, a number of 72 computational frameworks have been developed for performing *de novo* extraction of mutational 73 signatures (**Table 1**)<sup>15-25</sup>. Notably, the majority of existing *de novo* extraction tools (*i*) 74 predominately support the simplest mutational classification, viz., SBS-96 which encompasses single base substitutions with their immediate 5' and 3' sequence context<sup>2</sup>; *(ii)* lack automatic 75 76 selection for the number of mutational signatures; (iii) do not identify a robust solution leading to 77 different results following re-analysis of the same dataset; (iv) require pre-selection of a large 78 number of priors and/or hyperparameters; (v) do not decompose de novo signatures to the set of

79	reference COSMIC signatures <sup>11</sup> . Importantly, there has been no extensive benchmark of the
80	existing tools for <i>de novo</i> extraction leading to uncertainty in regard to their performance.
81	

82	To address these limitations, here, we present SigProfilerExtractor – a reference tool for <i>de novo</i>
83	extraction of mutational signatures. SigProfilerExtractor allows analysis of all types of
84	mutational classifications, performs automatic selection of the number of signatures, yields
85	robust solutions, requires only minimum setup, and decomposes de novo extracted signatures to
86	known COSMIC signatures. A comprehensive benchmark including 2,879 applications of
87	SigProfilerExtractor and ten other tools across a total of 33 distinct scenarios reveals that
88	SigProfilerExtractor is robust to noise and it outperforms all other computational tools for de
89	novo extraction of mutational signatures (Supplementary Tables 1–3). Applying
90	SigProfilerExtractor to the recently published set of 2,778 whole-genome sequenced cancers
91	from the Pan-Cancer Analysis of Whole Genomes (PCAWG) project <sup>26</sup> elucidates three novel
92	signatures that were not found in the original PCAWG analysis of mutational signatures <sup>11</sup> . Two
93	of the signatures are confirmed in independent cohorts and a putative etiology of tobacco-
94	associated mutagenesis is attributed to one of these signatures.
05	

## 96 **RESULTS**

### 97 Overview of SigProfilerExtractor and its implementation

- 98 SigProfilerExtractor is implemented as a Python package, with an R wrapper, allowing users to
- 99 run it in both Python and R environments:
- 100 <u>https://github.com/AlexandrovLab/SigProfilerExtractor</u>. The tool is also extensively
- 101 documented including a detailed Wiki page: <u>https://osf.io/t6j7u/wiki/home/</u>. By default, the tool
- 102 requires only a single parameter the input dataset containing the mutational catalogues of
- 103 interest. SigProfilerExtractor supports most commonly used formats outputted by variant calling
- 104 algorithms (e.g., VCF and MAF), which are internally converted to a matrix, M, by
- 105 SigProfilerMatrixGenerator<sup>2</sup>. SigProfilerExtractor can also be applied to a text file containing a

106 matrix, *M*, thus supporting nonnegative matrix factorization for any custom matrix dataset. By

- 107 default, the tool decomposes the matrix *M* searching for an optimal solution between 1 and 25
- 108 mutational signatures (Figure 1*a*). For each decomposition, SigProfilerExtractor performs 500
- 109 independent factorizations and, for each repetition, the matrix *M* is first Poisson resampled and
- 110 normalized and, subsequently, factorized with the multiplicative update NMF algorithm<sup>3</sup> by
- 111 minimizing an objective function based on the Kullback–Leibler divergence measure<sup>27</sup> (Figure
- 112 **1b**). Custom partition clustering, that utilizes the Hungarian algorithm<sup>28</sup> for comparing different
- 113 repetitions, is applied to the 500 factorizations to identify stable solutions<sup>29</sup> (Figure 1*b*).
- 114 Specifically, SigProfilerExtractor selects the centroids of stable clusters as optimal solutions,
- 115 thus, making these solutions resistant to fluctuations in the input data and to the lack of
- 116 uniqueness of NMF due to the potential existence of multiple convergent stationary points in the
- 117 solution<sup>30</sup>. Lastly, when applicable, the optimal set of *de novo* signatures are matched to the set

118	of reference COSMIC mutational signatures (Figure 1c) with any <i>de novo</i> signature reported as
119	novel when it cannot be decomposed by a combination of known COSMIC signatures.

# 121 Framework for benchmarking tools for de novo extraction of mutational signatures

122 To allow comprehensive benchmarking of tools for *de novo* extraction of mutational signatures, 123 more than 200,000 synthetic cancer genomes were generated with known ground-truth 124 mutational signatures (Supplementary Note 1). These synthetic data included 32 distinct 125 noiseless scenarios and one scenario with five different levels of noise. Each scenario contained 126 between 3 and 40 known signatures operative in 200 to 3,000 simulated cancer genomes 127 (Supplementary Tables 1–3). Some of the scenarios were generated up to 20 times to account 128 for variability in the simulated data. The majority of noiseless scenarios (20/32) were based on 129 SBS-96 mutational classification; 12 scenarios based on extended mutational classifications, *i.e.*, 130 matrices with more than 96 mutational channels, were also included (Supplementary Table 3). 131 To avoid bias in evaluating each tool's performance, three sets of SBS-96 mutational signatures 132 were used for generating the synthetic data: (i) COSMICv3 reference signatures<sup>11</sup>; (ii) SA signatures previously extracted by SignatureAnalyzer<sup>11</sup>; and *(iii)* randomly generated signatures. 133 134 For presentation simplicity, scenarios were labeled based on their complexity as easy, medium, 135 or hard. Easy scenarios were generated using  $\leq 5$  signatures and provide a good indication of each 136 tool's performance on approximately 7.4% of human cancer types (e.g., pediatric brain tumors). 137 Medium scenarios contained 11 to 21 signatures and biologically reflect 15.9% of cancer types 138 (e.g., cervical cancer). Hard scenarios have more than 25 signatures and reflect 59.5% of human 139 cancer types (e.g., breast, lung, liver, etc.) as well as pan-cancer datasets. In addition to the 32

140	noiseless scenarios, one SBS-96 scenario with five different levels of noise (average noise per
141	sample ranging between 0% and 10%) was included in the benchmark (Supplementary Note 1).
142	

- 143 To compare the performance between different tools for *de novo* extraction of mutational
- signatures, we developed a standard set of evaluation metrics (Supplementary Figure 1).
- 145 Specifically, each *de novo* extracted signature is classified as either a *true positive* (TP), *false*
- 146 positive (FP), or false negative (FN) signature. An extracted signature is considered TP if it
- 147 matches one of the ground-truth signatures above a cosine similarity threshold of 0.90. In

148 contrast, a signature is classified as FP when it has a maximum cosine similarity below 0.90 with

all ground-truth signatures. Lastly, FN signatures are ground-truth signatures that were not

150 detected in the data. These standard metrics allow calculating each tool's precision, sensitivity,

- 151 and F<sub>1</sub> score. Precision is defined as  $\frac{TP}{TP+FP}$ , sensitivity as  $\frac{TP}{TP+FN}$ , and F<sub>1</sub> score is the harmonic
- 152 mean of the precision and sensitivity:  $2 * \frac{Precision * Sensitivity}{Precision + Sensitivity}$
- 153

#### 154 Benchmarking SigProfilerExtractor and ten other tools using SBS-96 noiseless data

155 SigProfilerExtractor and ten other tools (Table 1) were first applied to all noiseless scenarios 156 based on the SBS-96 mutational classification. Each tool was applied to each scenario by using 157 its suggested method for selecting the number of operative signatures and, with the exception of 158 SignatureAnalyzer which lacks this capability, by forcing each tool to extract the known number 159 of ground-truth signatures. Results from the suggested approach reflect the expected outcome 160 from running a tool on an unknown dataset, while results from the forced approach allow 161 understanding limitations in each tool's implementation. Our evaluation reveals that most tools 162 are able to successfully extract mutational signatures from easy scenarios with the majority of  $F_1$ 

163 scores between 0.90 and 1.00 (Figure 2a). This is perhaps unsurprising as many of these tools 164 used synthetic data with  $\leq$ 5 signatures to evaluate their performance in the respective original publications<sup>15-25</sup>. In contrast, medium scenarios have proven to be a challenge for the majority of 165 166 tools with only SigProfilerExtractor and SignatureAnalyzer exhibiting an F<sub>1</sub> score above 0.90. 167 All tools had worst performance for the hard set of scenarios with F<sub>1</sub> scores below 0.70; only 168 SigProfilerExtractor had an F<sub>1</sub> score above 0.85 (Figure 2*a*). 169 170 To evaluate whether the type of ground-truth signatures affects the *de novo* extraction, we 171 compared the ratio of  $F_1$  scores ( $rF_1$ ) from scenarios generated using COSMIC, SA, or random 172 signatures (Figure 2b). Most tools had similar performance ( $rF_1 \approx 1$ ) between COSMIC and 173 random signatures and worst performance with SA signatures ( $rF_1 < 1$ ). SomaticSignatures was an

exception as it performed well on random signatures but had similarly suboptimal performance

175 on COSMIC and SA signatures. SigProfilerExtractor outperformed all other tools regardless of

176 whether the synthetic data were generated using COSMIC, SA, or random signatures

177 (Supplementary Table 1).

178

To examine the performance of *de novo* extraction between the suggested and forced selection of the total number of signatures, we evaluated  $rF_1$  across all medium and hard scenarios (**Figure 2***c*). SigProfilerExtractor exhibited almost identical  $F_1$  scores between the suggested and forced selection indicating a good performance of the automatic selection algorithm. Most other tools had similar  $F_1$  scores between the suggested and forced selection albeit with more variability across the different scenarios (**Figure 2***c*). For example, MutSpec had  $rF_1 \approx 1$  in both medium and hard scenarios indicating that MutSpec is performing worse than SigProfilerExtractor (**Figure** 

186	(2a) not because of its algorithm for selecting the total number of signatures but likely due to its
187	implementation of the utilized numerical factorization. SigneR (hard scenarios), SigMiner
188	(medium), and SigFit (all) had lower F1 scores for automatic solutions compared to forced
189	solutions (rF <sub>1</sub> <1), thus, indicating that their automatic approaches for selecting the total number
190	of signatures are not optimally performing (Figure $2c$ ). Surprisingly, EMu had higher $F_1$ scores
191	for automatic solutions in some hard scenarios. Considering the overall performance of EMu
192	(Figure 2 <i>a</i> ), this outcome likely reflects the lack of convergence during the minimization of the
193	EMu objective function for certain number of signatures in the hard scenarios.
194	
195	Overall, across all suggested extractions from noiseless medium and hard scenarios,
196	SigProfilerExtractor outperformed all other tools. SigProfilerExtractor was able to identify
197	between 7% and 25% more true positive signatures while yielding between 3.7-and 16-fold less
198	false positive signatures compared to the next six best performing tools: SignatureAnalyzer,
199	SigneR, MutationalPatterns, MutSpec, SomaticSignatures, and SignatureTools (Figure 2d and
200	Supplementary Table 1).
201	
202	Extended benchmarking of SigProfilerExtractor and the other six top performing tools
203	The reported comparisons for SBS-96 scenarios rely on a cosine similarity ≥0.90 for determining
204	TP signatures and <0.90 for determining FP signatures. Note that a cosine similarity $\geq$ 0.90 is
205	highly unlikely to happen purely by chance (p-value = $5.90 \times 10^{-9}$ ) as two random nonnegative
206	vectors are expected to have an average cosine similarity of 0.75 purely by chance <sup>31</sup> .
207	SigProfilerExtractor's performance does not depend on the specific value of the cosine similarity
208	threshold (Figure $3a$ ) as the tool consistently outperforms other bioinformatics approaches for

almost any value of the threshold above 0.80 (p-value: 0.057). Cosine similarity thresholds
below 0.80 were not explored as extracted signature may be similar to ground-truth signatures
purely by chance.

212

213 Additional benchmarking was performed by generating 12 scenarios simulated using between 3 214 and 30 signatures with an extended number of mutational channels (Supplementary Note 1). 215 SigProfilerExtractor and SignatureAnalyzer are the only two tools that support analysis of 216 custom size matrices and also provide GPU support (Table 1), thus, allowing analysis of data 217 with extended number of mutational channels within a reasonable timeframe. In contrast, all 218 other tools rely solely on CPU implementations with full runs expected to take many months for 219 each tool applied to these scenarios (Table 1). SigProfilerExtractor and SignatureAnalyzer 220 exhibited similar performance on the extended noiseless scenarios to that observed on SBS-96 221 noiseless scenarios. Overall, SigProfilerExtractor outperformed SignatureAnalyzer with average 222 F1 scores of 0.92 and 0.85, respectively (Supplementary Table 2). 223 224 To further compare SigProfilerExtractor with the other six top performing tools, we applied each 225 tool to a dataset with 30 ground-truth SBS-96 signatures operative in 1,000 genomes and random 226 noise between 0% and 10%. Analysis for each noise level was repeated 20 times to account for 227 any variability in the noise. SigProfilerExtractor, SomaticSignatures, MutSpec, 228 SignatureToolsLib were robust to noise with mostly unaffected performance (Figure 3b and 229 Supplementary Table 3). In contrast, SignatureAnalyzer, SigneR, and MutationalPatterns were 230 susceptible to noise (Figure 3b). For example, 2.5% noise reduced SignatureAnalyzer's  $F_1$  from 231 0.76 to 0.66 while 10% noise reduced its  $F_1$  to 0.07. Similarly, 10% noise reduced the  $F_1$  of

232 SigneR from 0.61 to 0.43 and the  $F_1$  of MutationalPatterns from 0.60 to 0.37.

233 SignatureAnalyzer's reduced performance on data with noise is due to its automated approach 234 for selecting total number of signatures. SignatureAnalyzer uses automatic relevance 235 determination<sup>32</sup> for selecting the number of signatures with this number increasing from 26 (no 236 noise; 30 ground-truth signatures) to 96 signatures (10% noise; Supplementary Table 3). In 237 contrast, SigneR and MutationalPatterns exhibit similar performance between forced and 238 suggested solutions on data with noise (Supplementary Table 3) indicating that their reduced 239 performance is likely due to the numerical implementation of their respective factorization 240 approaches. 241 242 SigProfilerExtractor outperformed all other tools regardless of the levels of noise. Simulations 243 with 5% noise reflect genomics datasets with  $\sim 0.95$  average sensitivity and precision of single 244 base substitutions, similar to the recently published PCAWG cohort which has 95% sensitivity 245 (90% confidence interval, 88–98%) and 95% precision (90% confidence interval, 71–99%)<sup>26</sup>. 246 For simulations with 5% noise, SigProfilerExtractor was able to identify between 20% and 50% 247 more true positive signatures while yielding more than 5-fold less false positive signatures 248 compared to the next six best performing tools: SignatureAnalyzer, SigneR, MutationalPatterns, 249 MutSpec, SomaticSignatures, and SignatureTools (Figure 3c and Supplementary Table 3). 250 251 Analysis of 2,778 whole-genome sequenced human cancers with SigProfilerExtractor 252 To demonstrate its ability to yield novel biological results, SigProfilerExtractor was applied to

the recently published set of 2,778 whole-genome sequenced cancers<sup>26</sup>. As previously done in

our original PCAWG analysis of mutational signatures<sup>11</sup>, extraction of mutational signatures was

255	performed within each cancer type as well as across all samples (Supplementary Data). In
256	addition to all previously detected signatures <sup>11</sup> , three novel mutational signatures were identified
257	in the PCAWG dataset: SBS92, SBS93, and SBS94 (Figure 4 and Supplementary Table 4).
258	
259	Signature SBS92 was found predominately in PCAWG bladder cancers; the signature was
260	characterized by T>C mutations with strong transcriptional strand bias consistent with damage
261	on purines for all types of single base substitutions (Figure 4a). Signature SBS92 was 9-fold
262	elevated (Figure 4d; p-value: 7.6 x 10 <sup>-3</sup> using Wilcoxon rank sum test) in bladder cancers of ever
263	smokers compared to never smokers in the PCAWG cohort. An almost identical signature was
264	identified by re-analyzing a recently published cohort of 88 whole-genome sequenced
265	microbiopsies of histologically normal urothelium <sup>33</sup> with the similarity extending to both
266	trinucleotide context and transcriptional strand bias (Figure 4a; cosine similarity: 0.98; p-value <
267	$10^{-256}$ ). Indeed, this signature was reported in the original publication and found to be enriched in
268	smokers <sup>33</sup> . In our analysis, SBS92 was found to be 3-fold elevated in the normal urothelium of
269	tobacco ever smokers compared to never smokers (Figure 4d; p-value: $8.3 \times 10^{-3}$ using
270	Wilcoxon rank sum test).

272 Signature SBS93 was identified almost exclusively in PCAWG stomach cancers. SBS93 was 273 characterized by T>C and T>G mutations with a strand bias consistent with damage on 274 pyrimidines for TpTpA contexts (mutated base underlined; Figure 4b). *De novo* extraction from 275 the Mutographs cohort of 552 whole-genome sequenced esophageal squamous cell carcinomas<sup>34</sup>, a cancer type not included in the PCAWG dataset<sup>26</sup>, identified an analogous mutational signature 276 277 with the similarity extending to both trinucleotide context and transcriptional strand bias (Figure

- 4b; cosine similarity: 0.88; p-value: 1.1 x 10<sup>-6</sup>). Signature SBS94 was found at high levels in a
- single colorectal PCAWG cancer with smaller contributions to another 8 colorectal cancers. The
- 280 pattern of SBS94 was characterized by C>A mutations with a strand bias indicative of damage
- 281 on guanine (Figure 4c). Validation of somatic mutations by visual inspection confirmed that
- 282 98% of mutations contributed by SBS94 are likely real. Signatures SBS93 and SBS94 did not
- associate with any of the available PCAWG metadata<sup>26</sup> and their etiologies remain unknown.

#### 285 **DISCUSSION**

286 The performed large-scale benchmarking demonstrates that SigProfilerExtractor outperforms ten

- 287 other tools for *de novo* extraction of mutational signatures for noiseless datasets as well as for
- 288 datasets containing matrices with different levels of random noise. Importantly,
- 289 SigProfilerExtractor generates almost no false positive signatures while still identifying a higher
- 290 number of true positive signatures when compared to any of the other tools (Figure 2d and
- 291 Figure 3c). De novo extraction of mutational signatures relies both on a factorization approach
- and on a model selection algorithm for determining the total number of operative signatures
- 293 (Figure 1). Benchmarking with forced model selection, where tools were required to extract the
- known number of ground-truth mutational signatures, reveals that SigProfilerExtractor's

factorization performs better when compared to the factorizations of other tools (Figure 2a and

296 Supplementary Tables 1-3). Similarly, benchmarking with suggested model selection, which

297 most closely matches analysis of a real dataset with unknown number of signatures, further

298 demonstrates SigProfilerExtractor's ability to reveal novel biological results (Figure 2a and

299 Supplementary Tables 1-3).

300

While our benchmarking evaluated ten additional tools, six of the ten tools internally rely on the
same computational engine. Maftools, MutationalPatterns, MutSpec, SignatureToolsLib,
SigMiner, and SomaticSignatures use the NMF R package<sup>35</sup> to perform their factorization (**Table**1), albeit with slightly different hyperparameters and, in some cases, distinct pre-processing of
the input matrix. Predictably, these six tools have similar performance across many of the
scenarios (**Supplementary Tables 1-3**). SigFit also uses a previously developed nonnegative
factorization method, *viz.*, Stan R package<sup>36</sup>. In contrast, EMu, SignatureAnalyzer, SigneR, and

308	SigProfilerExtractor provide original implementations of their factorization algorithms (Table
309	1). EMu was originally developed and tested on small datasets ( <i>e.g.</i> , 21 breast genomes) <sup>15</sup> and its
310	benchmarking performance is perhaps unsurprising considering the large number of synthetic
311	samples used in all scenarios. Surprisingly, the original implementations of SignatureAnalyzer
312	and SigneR were susceptible to noise, yielding high numbers of false-positive signatures (Figure
313	<b>3</b> <i>b</i> ).
314	

315 Six of the other ten tools did not provide an automatic approach for selecting the total number of 316 operative signatures in a dataset (Table 1). Instead, these tools offered methodologies for 317 manually selecting the optimal number of signatures bringing user-dependence and arbitrariness 318 in selecting solutions. EMu, SigFit, SignatureAnalyzer, SigMiner, SigneR, and 319 SigProfilerExtractor provided capabilities for automatically selecting the total number of 320 signatures. EMu and SigneR select the total number of signatures using Bayesian information 321 criterion (BIC)<sup>37</sup>, while SignatureAnalyzer and SigMiner utilize automatic relevance 322 determination  $(ARD)^{32}$ . SigFit's selection approach is based on the Elbow method<sup>38</sup>. 323 SigProfilerExtractor leverages a modified version of the NMFk selection approach which was 324 previously tested on more than 55,000 synthetic random matrices with pre-determined latent 325 factors and shown to outperform other model selection approaches<sup>39</sup>. Importantly, our 326 simulations demonstrate that SigProfilerExtractor's model selection is robust to noise while the 327 implemented BIC and ARD approaches are affected even by low levels of noise (Figure 3b). 328 329 In addition to outperforming ten other tools on simulated datasets, SigProfilerExtractor is able to

330 reveal additional biological results as demonstrated by identifying three novel signatures from

331 reanalysis of the PCAWG dataset. Importantly, SigProfilerExtractor identifies signature SBS92 332 (Figure 4) which is associated with tobacco smoking in whole-genome sequenced bladder 333 cancers and in whole-genome sequenced microbiopsies from normal bladder urothelium. The 334 strong transcriptional strand bias observed in SBS92 is indicative of an environmental mutagen 335 exposure that damages purines. Tobacco smoke is a complex mixture of at least 60 chemicals<sup>14</sup>, 336 many capable of causing damage on purines. Interestingly, our and other prior analyses of exome 337 sequenced bladder cancers from The Cancer Genome Atlas (TCGA) project<sup>14,40</sup> did not reveal 338 SBS92. Reanalysis of the set of TCGA bladder cancer exomes<sup>41</sup> with SigProfilerExtractor was 339 also unable to detect SBS92 (Supplementary Data). We suspect that the lack of SBS92 in the 340 TCGA bladder cancers was due to the use of exome sequencing; note that SBS92 is 341 predominately found in intergenic regions (Figure 4a) with most samples expected to have less 342 than 15 mutations from SBS92 in their exomes. To confirm this hypothesis, we downsampled the 343 whole-genome sequenced bladder cancers and the whole-genome sequenced microbiopsies from 344 normal bladder urothelium to exomes. SigProfilerExtractor's analysis of these downsampled 345 genomes was unable to detect SBS92 confirming that exome sequencing is insufficient to 346 identify signature SBS92 (Supplementary Data).

347

In summary, here we report SigProfilerExtractor – a computational tool for *de novo* extraction of mutational signatures. We demonstrate that SigProfilerExtractor outperforms ten other tools by conducting the largest benchmarking of bioinformatics approaches for extracting mutational signatures. Further, we apply SigProfilerExtractor to 2,778 whole-genome sequenced cancers and reveal several novel mutational signatures including a signature putatively attributed to tobacco smoking mutagenesis in bladder cancer and in normal bladder epithelium.

### **355 ONLINE METHODS**

### 356 Computational implementation of SigProfilerExtractor and its seven modules

357 The implementation of SigProfilerExtractor can be separated into seven distinct modules which 358 are packaged together into a single bioinformatics tool. *Module 1* processes the initial input data, 359 which can be provided as either a mutational catalogue containing a set of somatic mutations or a 360 mutational matrix. Module 2 is responsible for resampling and normalization of the mutational 361 matrix prior to performing nonnegative matrix factorization. Module 3 performs matrix 362 factorization using nonnegative matrix factorization with multiple replicates. Module 4 utilizes 363 custom clustering to derive consensus solutions and to perform model selection. Module 5 364 decomposes the derived set of *de novo* signatures to a set of previously derived COSMIC 365 signatures. Module 6 is responsible for calculating the activities of different signatures in 366 individual samples. *Module* 7 handles the extensive outputting and plotting of the different 367 analysis performed by SigProfilerExtractor. In principle, each of these modules allows extensive 368 customization. SigProfilerExtractor provides a seamless integration of these seven modules that 369 allows using them in an orchestrated and preconfigured manner with little input from a user.

370

#### 371 Module 1: Processing of input mutational catalogues or input mutational matrices

372 SigProfilerExtractor deciphers mutational signatures from a mutational matrix *M* with *t* rows 373 and *n* columns; rows represent mutational channels while columns reflect individual cancer 374 samples (Figure 1*a*). The value of each cell in the matrix, *M*, corresponds to the number of 375 somatic mutations from a particular mutational channel in a given sample. The mutational matrix 376 can be provided as a text file with the first column containing the names of the mutational 377 channels and the first row containing the names of the examined samples. Alternatively, users

can provide a mutational catalogue of somatic mutations in a commonly used format (*e.g.*, VCF,
MAF, *etc.*) and this mutational catalogue will be internally converted into the appropriate
mutational matrix by SigProfilerMatrixGenerator<sup>2</sup>.

381

# 382 Module 2: Resampling of the input mutational matrix and normalizing the resampled matrix

383 SigProfilerExtractor does not factorize the original input matrix. Rather, prior to performing 384 matrix factorization, SigProfilerExtractor performs independent Poisson resampling of the 385 original matrix for each replicate<sup>1</sup>. As such, the matrix factorized in each replicate is never the 386 same for a given value of k (Figure 1b). The resampling is performed to ensure that Poisson 387 fluctuations of the matrix do not impact the stability of the factorization results. Additional 388 normalization is performed after resampling to overcome potential skewing of the factorization 389 from any hypermutators. SigProfilerExtractor supports four standard normalization methods<sup>42</sup>: 390 (i) Gaussian mixture model (GMM) normalization (default); (ii) 100X normalization; (iii) log2 391 normalization; (iv) no normalization. No normalization does not perform any additional 392 transformation on the Poisson resampled matrix. In log2 normalization, the sum of each column 393 in the matrix is derived and logarithm with base 2 is calculated for each of these sums. Each cell 394 in a column of the matrix is multiplied by the log2 of the column-sum and subsequently divided 395 by the original column sum. In 100X normalization, the sum of each column in the matrix is 396 derived. For each column where the sum exceeds 100 times the number of mutational channels 397 (*i.e.*, 100 times the number of rows in the matrix), each cell in the column is multiplied by the 398 100 times the number of mutational channels and subsequently divided by the original column 399 sum. This normalization ensures that no sample has a total number of mutations above 100 times 400 the number of mutational channels. GMM normalization encompasses a two-step process. The

401 first step derives the normalization cutoff value in a data-driven manner using a Gaussian 402 mixture model (GMM). The second step normalizes the appropriate columns using the derived 403 cutoff value. The first step uses a GMM to separate the samples into two groups based on their 404 total number of mutations; the total number of mutations in a sample reflects the sum of a 405 column in the matrix. The group with larger number of samples is subsequently selected, and the 406 same process is applied iteratively until it converges. Convergence is achieved when the mean of 407 the two groups is separated by no more than four standard deviations of the larger group. A 408 cutoff value is derived as the average value plus two standard deviations from the total number 409 of somatic mutations in the last large group. If the derived cutoff value is below 100 times the 410 number of mutational channels, the cutoff value is adjusted to 100 times the number of mutational channels. For each column where the sum exceeds the derived cutoff value, each cell 411 412 in the column is multiplied by the cutoff value and subsequently divided by the original column 413 sum. Note that no normalization is performed if the means of the first two groups are not 414 separate by at least four standard deviations. In all cases, columns with a sum of zero, reflecting, 415 genomes without any somatic mutations, are ignored to avoid division by zero.

416

417

# 418 Module 3: Matrix Factorization Using Nonnegative Matrix Factorization with Replicates

By default, SigProfilerExtractor factorizes the matrix M with different ranks searching for an optimal solution between k=1 and k=25 mutational signatures. For each value of k, by default, the tool performs 500 independent nonnegative matrix factorizations of the normalized Poisson resampled input matrix. Thus, for each value of k, SigProfilerExtractor generates 500 distinct factorizations of normalized Poisson resampled matrices resulting into 500 different matrices S, 424 each matrix reflecting the patterns of the *de novo* mutational signatures, and 500 different 425 matrices A, each matrix reflecting the activities of the *de novo* mutational signatures (Figure 1b). 426 To perform each of these factorizations, SigProfilerExtractor utilizes a custom implementation of 427 the multiplicative update algorithm<sup>3</sup>. Specifically, SigProfilerExtractor initializes the S and A428 matrices in the first step of the factorization using either random initial conditions (default) or 429 one of the derivatives of nonnegative double singular vector decomposition<sup>43</sup>. 430 SigProfilerExtractor provides internal support for minimizing three different objective functions 431 based on: (i) generalized Kullback-Leibler updates (default); (ii) Euclidean updates; (iii) Itakura-432 Saito updates. By default, the tool performs all factorization using multithreading of central 433 processing units (CPUs) and also provides support for factorization using graphics processing units (GPUs) by leveraging PyTorch<sup>44</sup>. In all cases, by default, the implemented minimization 434 435 performs at least 10,000 iterations (also known as NMF updates or NMF multiplicative update 436 steps) with a maximum of 1,000,000 iterations. By default, the convergence tolerance of the algorithm is set to 10<sup>-15</sup>. Note that SigProfilerExtractor allows configuring all factorization 437 438 parameters.

439

#### 440 Module 4: Custom partition clustering and performing model selection

The previously described *Module 3* generates a number of sets with each set containing, by default, 500 different matrices S, where each matrix reflects the patterns of *de novo* mutational signatures for a particular factorization of a normalized Poisson resampled matrix. One set, containing 500 different matrices S, is generated for each of the interrogated total number of operative signatures, k, with a default range for k between 1 and 25 signatures. For each value of k, *Module 4* first performs custom clustering of the S matrices and, subsequently, applies a

447 modified version of the NMFk model selection approach to select the optimal value of  $k^{39}$ 448 (Figure 1b). Specifically, for each value of k, the clustering is initialized with k random 449 centroids. One of the S matrices is randomly chosen, and its columns matched to the most similar 450 centroids with no two columns assigned to the same cluster. The process is repeated until the 451 columns of all S matrices in the set are assigned to their respective clusters. SigProfilerExtractor implements the Hungarian algorithm<sup>28</sup> to pair consensus vectors from two matrices (*i.e.*, cluster 452 453 centroids and mutational signature from a matrix  $\boldsymbol{S}$ ; the Hungarian algorithm maximizes the 454 total cosine similarities of all paired vectors between two matrices<sup>28</sup>. After assigning all columns 455 to a cluster, the centroids of each cluster are recalculated by evaluating the average of all 456 columns/vectors in a cluster. This process continues iteratively until the average silhouette coefficient converges (*i.e.*, its value does not change by more than  $10^{-12}$ ). After convergence for a 457 458 given value of k, the centroids of the clusters are reported as consensus mutational signatures, an 459 overall reconstruction error is calculated for describing the original input matrix, M, and stability is calculated for each signature by computing the silhouette value<sup>45</sup> of the cluster corresponding 460 461 to that signature (Figure 1b). The silhouette value of a cluster measures the similarities of the 462 objects assigned to that cluster compared to any other cluster. Silhouette values range from -1.0 463 to +1.0 with values above zero indicating that, on average, objects have a higher similarity with 464 their own cluster compared to their nearest clusters. Note that signatures with low stability 465 correspond to a lack of uniqueness of the NMF due to Poisson resampling and/or to the potential 466 existence of multiple convergent stationary points in the NMF solution<sup>30</sup>.

467

468 Our custom clustering is performed for each of the interrogated total number of operative

469 signatures, k, with a default range for k between 1 and 25 signatures. After performing clustering,

for each value of k, one has derived: (i) the consensus set of mutational signatures; (ii) an overall
reconstruction error for describing the original input matrix; and (iii) stability value for each of
the identified consensus mutational signatures.

473

SigProfilerExtractor performs a solution selection based on the stability of signatures in a 474 475 solution and the ability of these signatures to reconstruct the original input matrix. By default, 476 SigProfilerExtractor will consider solutions stable if the signatures derived in the solution have 477 an average stability above 0.80 with no individual signature having stability below 0.20. To 478 reduce overfitting, the tool also measures the information gained from the extracted set of 479 signatures in each solution. SigProfilerExtractor compares, using Wilcoxon rank-sum tests, the 480 reconstruction errors across all samples from the stable solution with the greatest number of 481 signatures to the reconstruction errors across all samples from stable solutions with lower 482 number of signatures. Stable solutions with lower number of signatures are compared in a 483 decreasing order to their total number of signatures with comparison stopping if the Wilcoxon 484 rank-sum test yields a *p*-value below 0.05 (*i.e.*, reflecting that a solution does not describe the 485 original data as good as the stable solution with the greatest number of signatures). The stable 486 solution with lowest number of signatures and a Wilcoxon rank-sum test *p-value* above 0.05 is 487 selected as the optimal solution. If no solution has a Wilcoxon rank-sum test *p-value* above 0.05, 488 the stable solution with the greatest number of signatures is selected as the optimal solution. Note 489 that while SigProfilerExtractor selects an optimal solution, it outputs all the information 490 necessary to evaluate mutational signatures and their activities for all other stable and unstable 491 solutions.

#### 493 Module 5: Decomposing de novo extracted signatures to known COSMIC signatures

494 SigProfilerExtractor provides a module for decomposing each of the *de novo* extracted 495 mutational signatures to a set of previously derived signatures. By default, the tool decomposes each of the signatures in the optimal solution to a set of COSMICv3 reference signatures<sup>11</sup> with 496 497 support for signatures of single base substitutions (SBS), doublet base substitutions (DBS), and 498 small insertions and deletions (ID). Since the SBS COSMICv3 reference signatures were derived 499 under the SBS-96 classification<sup>2</sup>, any extended classification of single base substitutions (e.g., 500 SBS-288 and SBS-1536)<sup>2</sup> is first collapsed to the SBS-96 classification and, subsequently, 501 decomposed to the COSMICv3 reference signatures<sup>11</sup>. The decomposition functionality leverages nonnegative least square (NNLS) algorithm<sup>46</sup> as its main computational engine. A 502 503 mixture of addition and removal steps (add-remove functionality) were developed to estimate the 504 list of COSMIC signatures for a *de novo* signature. Specifically, for each *de novo* signature, a 505 COSMIC signature is iteratively added to a list of signatures used to explain the *de novo* 506 signature, NNLS is applied, and the signature which addition causes the greatest decrease of the 507 L2 error is selected. If this greatest decrease is more than a specific threshold (default value of 508 0.05) then the signature is included in the list of signatures used to explain the *de novo* signature. 509 The addition is immediately followed by a removal step. Each COSMIC signature in the list of 510 signatures used to explain the *de novo* signature are iteratively removed, NNLS is applied, and 511 the signature that causes the least decrease of the L2 error is selected. If this least decrease is less 512 than a specific threshold (default value of 1%) then the signature is removed from the list of 513 signatures used to explain the *de novo* signature. The addition and removal steps are iterated until 514 no signatures are added or removed from the list of signatures used to explain the *de novo* 515 signature. Several previously implemented rules for mutational signatures are incorporated by

516	default in the decomposition module <sup>11</sup> . Specifically, for signatures of single base substitutions:
517	(i) the list of signatures used to explain the <i>de novo</i> signature is initialized with clock-like
518	signatures SBS1 and SBS5; <sup>12</sup> (ii) biologically connected signatures are included as previously
519	done in Ref <sup>11</sup> ( <i>e.g.</i> , if SBS17a is included in the list then SBS17b is also included the list). The
520	decomposition module is highly customizable as it allows changing all default parameters as
521	well as adding additional new rules or removing existing rules for inclusion and exclusion of
522	particular signatures.

# 524 *Module 6: Evaluating activities of mutational signatures in individual samples*

525 De novo extracted and COSMIC derived signatures are refitted to individual samples using nonnegative least squares (NNLS)<sup>46</sup>. *Module 6* internally utilizes the add-remove functionality of 526 527 *Module 5* with each sample in the original matrix, *M*, being individually examined. For *de* 528 novo mutational signatures, all *de novo* signatures are initially added to the list of signatures used 529 to explain the sample and a removal step with a cutoff of 2% is applied. To assign COSMIC 530 signatures in a sample, the module first derives the set of *de novo* signatures in that sample. 531 Decomposition to the COSMICv3 signatures using *Module 5* is performed for each of the *de* 532 novo signatures and the identified COSMICv3 signatures are refitted using the add-remove 533 functionality with a removal and addition cutoffs set at 5%. Finally, the activity matrix is 534 constructed by combining the activity vectors generated for all samples in the dataset.

535

# 536 Module 7: Outputting and plotting of analysis results

537 All previous modules make use of *Module* 7 for outputting and plotting of the generated results.

538 It should be noted that SigProfilerExtractor provides extensive output for the interrogated total

539	number of operative signatures, $k$ , with a default range of $k$ between 1 and 25 signatures. For
540	each value of $k$ , SigProfilerExtractor outputs the set of operative <i>de novo</i> mutational signatures,
541	the activities of the operative signatures, and an extensive set of information related to individual
542	samples, individual de novo signatures, and the overall convergence of the factorization and
543	clustering. Module 7 also provides additional information when ran in debug mode. In addition
544	to outputting information, SigProfilerExtractor also generates a bouquet of plots both for each
545	value of $k$ as well as for the suggested optimal solution. SigProfilerExtractor utilizes all
546	previously implemented plots in SigProfilerPlotting <sup>2</sup> as well as includes a number of newly
547	developed plots.
548 549 550	Analysis of the genomics data from cancer and normal somatic tissues
551	For all examined cancer and normal somatic tissues, de novo extraction of mutational signatures
552	was performed with SigProfilerExtractor with default parameters using two distinct mutational
553	classifications: SBS-96 and SBS-288. The SBS-96 mutation classification incorporates the six
554	types of single base substitutions: C>A, C>G, C>T, T>A, T>C, and T>G. Each type of single
555	base substitution is further separated into 16 subtypes determined by the four possible bases 5'
556	and 3' adjacent to each mutated base. The SBS-288 mutation classification extends the SBS-96
557	mutation classification by adding additional information for each of the 96 subtypes.
558	Specifically, SBS-288 incorporates whether a single base substitution is in non-
559	transcribed/intergenic DNA, on the transcribed strand of a gene, or on the untranscribed strand of
560	the gene. De novo extraction was performed separately for all examined datasets. Specifically,
561	SigProfilerExtractor was applied: (i) to all 2,778 whole-genome sequenced cancers from the Pan-
562	Cancer Analysis of Whole Genomes project <sup>26</sup> ; (ii) to all samples in each of the 37 cancer types

563 of Pan-Cancer Analysis of Whole Genomes project<sup>26</sup> with each cancer type examined separately; 564 *(iii)* to all 88 whole-genome sequenced microbiopsies of histologically normal urothelium<sup>33</sup>; *(iv)* to the complete set of bladder cancers from  $TCGA^{41}$ ; (v) to exome downsampling of all bladder 565 566 whole-genome sequenced cancers from the Pan-Cancer Analysis of Whole Genomes project<sup>26</sup>; 567 (vi) to exome downsampling of all 88 whole-genome sequenced microbiopsies of histologically 568 normal urothelium<sup>33</sup>. In all cases, the mutational catalogues of each samples were taken from the 569 respective original publications. The results from all performed *de novo* extractions can be found 570 in Supplementary Data. Downsampling of a whole-genome sequenced sample to a whole-571 exome was performed using SigProfilerMatrixGenerator<sup>2</sup>. 572 573 Additional approaches for miscellaneous analysis 574 Synthetic scenarios were labeled as easy, medium, and hard based on the number of operative 575 signatures in each scenario. Based on our most recent analysis of mutational signatures in 82 576 cancer types<sup>11</sup>, approximately 7.4% of human cancer types have 5 or less signatures (reflected in 577 simulations of easy scenarios), 15.9% have 11 to 21 signatures (medium scenarios), and 59.5% 578 have 25 or more signatures (hard scenarios). Note that 17.2% of cancer types have either 579 between 5 and 10 signatures or between 22 and 24 signatures. 580 581 Cosine similarity was used to compare the profiles of different mutational signatures. P-values 582 can be attributed to cosine similarities based on a null hypothesis of uniform random distribution 583 of nonnegative vectors<sup>31</sup>.

585	Briefly, the prevalence of somatic mutations in a whole-exome sample was calculated based on
586	the identified mutations in protein coding genes and assuming that an average whole-exome has
587	sufficient coverage of 30.0 megabase-pairs in protein coding genes. The prevalence of somatic
588	mutations in a whole-genome sample was calculated based on all identified mutations and
589	assuming that an average whole-genome has sufficient coverage of 3.00 gigabase-pairs.
590	
591	All methods related to the generation of the benchmarking scenarios and the application of the
592	different tools to these scenarios can be found in Supplementary Note 1.

bioRxiv preprint doi: https://doi.org/10.1101/2020.12.13.422570; this version posted December 13, 2020. The copyright holder for this preprint (which was not certified by peer review) is the author/funder. All rights reserved. No reuse allowed without permission.

# 594

## 595 **TABLES**

	Input	Platform	Factorization Approach			Selection Approach			Supported Contexts		COSMIC
Tool Name			Method	Computational Engine	GPU	Manual	Automatic	Automatic Algorithm	Mutational Catalogue Support	Plotting	Comparison
EMu <sup>15</sup>	Matrix	C++	EM	Original implementation <sup>15</sup>	No	Yes	Yes^	BIC <sup>37</sup>	SBS-96	No	No
Maftools <sup>16</sup>	Matrix MAF	R-Bioconductor	NMF	NMF R package <sup>35</sup>	No	Yes	No	-	SBS-96	SBS-96	1-to-1
MutationalPatterns <sup>17</sup>	Matrix VCF	R-Bioconductor	NMF	NMF R package <sup>35</sup>	No	Yes	No	-	SBS-96 SBS-192	SBS-96 SBS-192	1-to-1
MutSpec <sup>18</sup>	Matrix VCF Custom	Galaxy Perl R	NMF	NMF R package <sup>35</sup>	No	Yes	No	-	SBS-96 SBS-192	SBS-96 SBS-192	1-to-1
SigFit <sup>19</sup>	Matrix	R	Bayesian Inference	Stan R package <sup>36</sup>	No	Yes	Yes^	Elbow method <sup>38</sup>	SBS-96	SBS-96 SBS-192	1-to-1
SigMiner <sup>20</sup>	Matrix MAF	R	[automatic] Bayesian NMF [manual] NMF	[automatic] SignatureAnalyzer implementation <sup>21</sup> [manual] NMF R package <sup>35</sup>	No	Yes^	Yes	ARD <sup>32</sup>	SBS-96 DBS-78 ID-83	Generic	1-to-1
SignatureAnalyzer <sup>21,22</sup>	Matrix MAF	R [CPU] <sup>18</sup> Python [GPU] <sup>19</sup>	Bayesian NMF	Original implementation <sup>21,22</sup>	Yes	No	Yes	ARD <sup>32</sup>	SBS-96 DBS-78 ID-83	SBS-96 DBS-78 ID-83	1-to-1
SignatureToolsLib <sup>23</sup>	Matrix VCF Custom	R	NMF	NMF R package <sup>35</sup>	No	Yes	No	-	SBS-96 DBS-78 ID-83 SV-32	SBS-96 SV-32 Generic	No
SigneR <sup>24</sup>	Matrix VCF	R-Bioconductor C++	Bayesian NMF	Original implementation <sup>24</sup>	No	Yes	Yes^	BIC <sup>37</sup>	SBS-96	SBS-96	No
SigProfilerExtractor	Matrix VCF MAF Custom	Python R wrapper	NMF	[current report] Original implementation	Yes	Yes	Yes^	NMFk <sup>39</sup>	SBS-96 DBS-78 ID-83 Others <sup>2</sup> Any	SBS-96 DBS-78 ID-83 SV-32 Others <sup>2</sup> Generic	1-to-many
SomaticSignatures <sup>25</sup>	Matrix VCF	R-Bioconductor	NMF PCA	NMF R package <sup>35</sup> pcaMethods R package <sup>47</sup>	No	Yes	No	-	SBS-96	SBS-96	No

596

# 597 Table 1: Overview of bioinformatics tools for *de novo* extraction of mutational signatures.

598 Tools are ordered alphabetically. Notations: ^ denotes the default approach for selecting the total

599 number of signatures when a tool supports both manual and automatic selection; 1-to-1 refers to

600 one *de novo* signature being matched with exactly one COSMIC signature; 1-to-many refers to

- 601 one *de novo* signature being matched with a combination of one or more COSMIC signatures.
- 602 Abbreviations: MAF: mutation annotation format; VCF: variant call format; EM: expectation-
- 603 maximization algorithm; NMF: nonnegative matrix factorization; ARD: automatic relevance
- 604 determination; BIC: Bayesian information criterion; COSMIC: catalogue of somatic mutations in
- 605 cancer; SBS: single base substitutions; DBS: doublet base substitutions; ID: small insertions and
- 606 deletions; SV: structural variants.

### 608 FIGURE LEGENDS

609 Figure 1. Overview of SigProfilerExtractor. (a) SigProfilerExtractor's general workflow is 610 outlined starting from an input of somatic mutations and resulting in an output of *de novo* 611 mutational signatures. An example is shown for a solution with three *de novo* signatures. 612 Somatic mutations are first converted into a mutational matrix. Subsequently, the matrix is 613 factorized with different ranks using nonnegative matrix factorization. Model selection is applied 614 to identify the optimal factorization rank based on each solution's stability and its reconstruction 615 of the original data. (b) Schematic representation for an example decomposition with a 616 factorization rank of k=3. By default, SigProfilerExtractor performs 500 independent 617 nonnegative matrix factorizations with the matrix *M* being Poisson resampled and normalized 618 (denoted by ^) prior to each factorization. Partition clustering of the 500 factorizations is used to 619 evaluate the factorization stability rank, measured in silhouette values; clustering can also be 620 presented as two-dimensional projections revealing more similar mutational signatures as shown 621 for the three example signatures. The centroid of the clustered solutions (denoted by -) is 622 compared to the original matrix M. (c) All identified de novo signatures are matched to a 623 combination of known COSMIC mutational signatures. An example is given for *de novo* 624 extracted signature SBS96B which matches a combination of COSMIC signatures SBS1, SBS2, 625 and SBS13.

626

## 627 Figure 2. Benchmarking of bioinformatics tools for *de novo* extraction of mutational

628 signatures using SBS-96 noiseless scenarios. (a) Average precision (x-axes), sensitivities (y-

629 axes), and F<sub>1</sub> scores (harmonic mean of precision and sensitivity; red curves) are shown across

630 the three types of scenarios. Different tools are displayed using circles and triangles with

631 different colors. Circles are used to display results for suggested model selection, which most 632 closely matches analysis of a real dataset. Triangles are used to display results for forced model 633 selection, where tools were required to extract the known total number of ground-truth 634 mutational signatures. All triangles are located on the diagonal as the forced model selection results in equal numbers of false positive and false negative signatures. (b) Evaluating the effect 635 636 of ground-truth signatures on the *de novo* extraction by different tools (x-axes). Ratio of F<sub>1</sub> 637 scores (y-axes) with confidence intervals were calculated for medium complexity scenarios 638 simulated using COSMIC, SA, or random signatures. Ratio of approximately 1.00 indicates a 639 similar performance between different types of signatures. (c) Evaluating the performance of de 640 *novo* extraction between suggested and forced selection for different tools (x-axes). Ratio of  $F_1$ 641 scores (y-axes) with confidence intervals were calculated for all medium and hard scenarios. 642 Ratio of approximately 1.00 indicates a similar performance between suggested and forced 643 model selection. (d) Summary of the performance for the top seven tools on medium and hard 644 SBS-96 noiseless scenarios with suggested model selection. Y-axes reflect  $F_1$  score (left plot), 645 sensitivity (middle plot), and false discovery rate (right plot), respectively. Results from 646 SignatureAnalyzer are not displayed in panels (a), (b), and (c) for forced model selection as 647 SignatureAnalyzer does not support predefined/forced solution with a specific total number of 648 signatures.

649

Figure 3. Additional evaluations of the top seven bioinformatics tools for *de novo* extraction
of mutational signatures. (a) Average F<sub>1</sub> scores for the top seven tools based on different
thresholds for cosine similarity in suggested medium and hard scenarios; thresholds for cosine
similarity are used for determining true positive signatures (Supplementary Figure 1). X-axes

654	reflect the cosine similarity thresholds, while the Y-axes correspond to the average F1 scores
655	corresponding to cosine similarity thresholds. (b) Precision and sensitivity of the top seven tools
656	for SBS-96 scenarios with different levels of noise. Noise levels reflect the average number of
657	somatic mutations in a cancer genome affected by additive white Gaussian noise; for example,
658	1% noise corresponds to approximately 1% of mutations in a sample being due to noise. (c)
659	Summary of the performance of the top seven tools on SBS-96 scenarios with 5% noise. Y-axes
660	reflect F <sub>1</sub> score (left plot), sensitivity (middle plot), and false discovery rate (right plot),
661	respectively.
662	
663	Figure 4. Novel signatures identified in the PCAWG cohort of 2,778 whole-genome
664	sequenced cancers. Mutational signatures are displayed using 96-plots. Single base substitutions
665	are shown using the six subtypes of substitutions: C>A, C>G, C>T, T>A, T>C, and T>G.

666 Underneath each subtype are 16 bars reflecting the sequence contexts determined by the four 667 possible bases 5' and 3' to each mutated base. Additional information whether mutations from a 668 signature are in non-transcribed/intergenic DNA, on the transcribed strand of a gene, or on the 669 untranscribed strand of the gene is provided adjacent to the 96 plots. (a) Mutational profile of 670 signature SBS92 derived from the PCAWG cohort (top). Confirmation of the profile of signature 671 SBS92 (bottom) by analysis of an independent whole-genome sequenced set of microbiopsies of histologically normal urothelium<sup>33</sup>. (b) Mutational profile of signature SBS93 derived from the 672 673 PCAWG cohort (top). Confirmation of the profile of signature SBS93 (bottom) by analysis of an 674 independent whole-genome sequenced set of esophageal squamous cell carcinomas<sup>34</sup>. (c) 675 Mutational profile of signature SBS94 derived from the PCAWG cohort. Signature SBS94 was 676 not identified in any additional independent cohort. (d) Bars are used to display average values

- 677 for numbers of somatic substitutions per megabase (Mb) attributed to signature SBS92 in bladder
- 678 cancer and normal bladder urothelium. Green bars represent never smokers, whereas blue bars
- 679 correspond to ever smokers. Error bars correspond to 95% confidence intervals. Each p-value is
- 680 based on a Wilcoxon rank sum test.
- 681

bioRxiv preprint doi: https://doi.org/10.1101/2020.12.13.422570; this version posted December 13, 2020. The copyright holder for this preprint (which was not certified by peer review) is the author/funder. All rights reserved. No reuse allowed without permission.

# 682 SUPPLEMENTARY INFORMATION

#### 683 Supplementary Figure 1. Standard set of performance metrics used for benchmarking all

- 684 bioinformatics tools. An example demonstrating the derivation of *true positive* (TP), *false*
- 685 positive (FP), or false negative (FN) signatures for a tool applied to a synthetic dataset generated
- using 6 ground truth signatures (termed, Ground Truth Signatures 1 through 6). The tool extracts
- 687 4 signatures (termed, Extracted Signatures A through D). In this example, an extracted signature
- 688 is considered a true positive if it matches one of the ground-truth signatures with a cosine
- 689 similarity threshold of at least 0.90.
- 690

# 691 Supplementary Table 1. Detailed performance metrics after applying each tool across all

692 SBS-96 noiseless synthetic scenarios. Performance metrics are calculated as per Supplementary

693 Figure 1. An extracted signature is considered a true positive if it matches one of the ground-

truth signatures with a cosine similarity threshold of at least 0.90.

- 695
- 696 Supplementary Table 2. Detailed performance metrics after applying the seven best

697 performing tools across SBS-96 synthetic scenarios with different levels of noise.

698 Performance metrics are calculated as per *Supplementary Figure 1*. An extracted signature is

considered a true positive if it matches one of the ground-truth signatures with a cosine similaritythreshold of at least 0.90.

701

# 702 Supplementary Table 3. Detailed performance metrics of applying SigProfilerExtractor

703 and SignatureAnalyzer to extended synthetic scenarios. Performance metrics are calculated

704	as per Supplementary Figure 1. An extracted signature is considered a true positive if it matches
705	one of the ground-truth signatures with a cosine similarity threshold of at least 0.90.
706	
707	Supplementary Table 4. Profiles of three novel mutational signatures identified in the
708	PCAWG cohort of 2,778 whole-genome sequenced cancers. The profiles of the novel
709	mutational signatures are reported using the SBS-288 classification which incorporates the
710	trinucleotide context and strand information (intergenic region, untranscribed strand, or
711	transcribed strand) for each type of single base substitution. The SBS-288 classification can be
712	easily collapsed to the commonly used SBS-96 classification.
713	
714	Supplementary Note 1. Detailed description of the performed benchmarking. The
715	supplementary note provides extensive details about each of the generated synthetic scenarios as
716	well as about applying each of the tools to these scenarios. The results from applying all tools to
717	all scenarios, including appropriate input and out files, can be found in Supplementary Data.
718	
719	Supplementary Data
720	All results from the benchmarking with synthetic datasets, including the appropriate input used
721	to run each of the tools as well as the output generated by each of the tools, can be found at:
722	ftp://alexandrovlab-ftp.ucsd.edu/pub/publications/Islam_et_al_SigProfilerExtractor/Benchmark/.
723	
724	All results from the <i>de novo</i> extraction of mutational signatures from the PCAWG dataset can be
725	found at: <u>ftp://alexandrovlab-</u>
726	ftp.ucsd.edu/pub/publications/Islam_et_al_SigProfilerExtractor/PCAWG_Reanalysis/.

- All results from the *de novo* extraction of mutational signatures for confirming the patterns of the
- novel signatures for additional datasets can be found at: <u>ftp://alexandrovlab-</u>
- 730 ftp.ucsd.edu/pub/publications/Islam et al SigProfilerExtractor/Confirmation of Novel Signatu

731 <u>res/</u>.

- 732
- 733 All results from the *de novo* extraction of mutational signatures from downsampling of whole-
- genome sequenced samples to whole-exomes can be found at: <u>ftp://alexandrovlab-</u>
- 735 <u>ftp.ucsd.edu/pub/publications/Islam et al SigProfilerExtractor/Downsampling of whole geno</u>
- 736 <u>mes/</u>
- 737

### 738 ACKNOWLEDGEMENTS

- 739 The authors would like to thank Allan Balmain (UC San Francisco) for the many useful
- 740 discussions as well as Ville Mustonen (University of Helsinki) and Israel Tojal Da Silva (A.C.
- 741 Camargo Cancer Center) for help in configuring EMu and SigneR, respectively. This work was
- supported by Cancer Research UK Grand Challenge Award C98/A24032 (LBA, PB, and MRS),
- 743 Wellcome grant reference 206194 (MRS), and US National Institute of Health grants
- R01MH116281-01A1 (BSA) and R01ES030993-01A1 (LBA). This work was also supported by
- 745 Singapore National Medical Research Council grants NMRC/CIRG/1422/2015 and MOH-
- 746 000032/MOHCIRG18may-0004 and the Singapore Ministry of Health via the Duke-NUS
- 747 Signature Research Programmes. LBA is an Abeloff V Scholar and he is supported by an Alfred
- 748 P. Sloan Research Fellowship. Research at UC San Diego was also supported by a Packard
- 749 Fellowship for Science and Engineering to LBA. AJG was funded by a postdoctoral fellowship
- 750 (grant nr. P2BSP3\_178591). NP receives funding through the Cancer Research UK Clinician
- 751 Scientist Fellowship scheme and is supported by University College London Cancer Institute.
- 752 Research at Los Alamos National Laboratory was conducted under Contract No.
- 753 89233218CNA000001 by the U.S. Department of Energy's National Nuclear Security
- 754 Administration and supported by Laboratory Directed Research and Development (LDRD) grant
- 755 20190020DR (BSA). CDS is supported by the GEM consortium and acknowledges funding for
- this work through a Cancer Research UK travel grant. The funders had no roles in study design,
- 757 data collection and analysis, decision to publish, or preparation of the manuscript.
- 758
- 759
- 760

# 761 AUTHOR CONTRIBUTIONS

- 762 LBA and SMAI designed both SigProfilerExtractor's methodology and the performed analyses
- 763 with help from NP, JZ, DJA, IM, BSA, LH, DCW, MTL, PB, MRS, and SGR. SMAI developed
- 764 SigProfilerExtractor with help from MV, ENB, YH, CDS, RV, and JW. All synthetic
- 765 benchmarking datasets were generated by YW and SGR. SMAI documented
- 766 SigProfilerExtractor and performed the benchmarking of all tools on synthetic data with help
- 767 from MDG, MB, BO, AK, and AA. Additional validations, confirmations, and applications of
- 768 SigProfilerExtractor to real and synthetic datasets were performed by SMAI, SM, SS, YRL, NS,
- 769 LR, TZ, AJG, YH, CDS, and SWB. LBA directed the overall research and wrote the manuscript
- with help from SMAI and input from all other authors. All authors read and approved the final

771 manuscript.

772

# 773 COMPETING INTERESTS

- 774 MV is an employee of NVIDIA corporation. All other authors declare no competing interests.
- 775

# 776 TOOL AVAILABILITY

777 SigProfilerExtractor and all its modules are open source and freely available for use under the

- permissive 2-clause BSD license. SigProfilerExtractor and its modules are implemented in
- 779 Python with an R wrapper package allowing users to run the tool from an R environment.
- 780 SigProfilerExtractor can be installed using the PyPI package manager from
- 781 <u>https://pypi.org/project/SigProfilerExtractor/</u> or downloaded from GitHub from
- 782 <u>https://github.com/AlexandrovLab/SigProfilerExtractor</u>. The R version of the tool can be
- 783 downloaded from <u>https://github.com/AlexandrovLab/SigProfilerExtractorR</u>. A detailed wiki

- 784 page including installation, usage, and explanation of result is provided at
- 785 <u>https://osf.io/t6j7u/wiki/home/</u>. SigProfilerExtractor is compatible with Windows, Linux, Unix,
- and macOS operating systems.

# 788 **REFERENCE**

789 790	1	Alexandrov, L. B., Nik-Zainal, S., Wedge, D. C., Campbell, P. J. & Stratton, M. R. Deciphering signatures of mutational processes operative in human cancer. <i>Cell Rep</i> <b>3</b> ,
791		246-259, doi:10.1016/j.celrep.2012.12.008 (2013).
792	2	Bergstrom, E. N. et al. SigProfilerMatrixGenerator: a tool for visualizing and exploring
793		patterns of small mutational events. BMC Genomics 20, 685, doi:10.1186/s12864-019-
794		6041-2 (2019).
795	3	Lee, D. D. & Seung, H. S. Learning the parts of objects by non-negative matrix
796	-	factorization. <i>Nature</i> <b>401</b> , 788-791, doi:10.1038/44565 (1999).
797	4	Févotte, C. & Cemgil, A. T. in 2009 17th European Signal Processing Conference.
798		1913-1917.
799	5	Dempster, A. P., Laird, N. M. & Rubin, D. B. Maximum Likelihood from Incomplete
800	-	Data Via the EM Algorithm. Journal of the Royal Statistical Society: Series B
801		(Methodological) <b>39</b> , 1-22, doi:10.1111/j.2517-6161.1977.tb01600.x (1977).
802	6	Suri, P. & Roy, N. R. in 2017 3rd International Conference on Computational
803	Ũ	Intelligence & Communication Technology (CICT). 1-5.
804	7	Alexandrov, L. B. Understanding the origins of human cancer. <i>Science</i> <b>350</b> , 1175,
805		doi:10.1126/science.aad7363 (2015).
806	8	Alexandrov, L. B. <i>et al.</i> Signatures of mutational processes in human cancer. <i>Nature</i> <b>500</b> ,
807	-	415-421, doi:10.1038/nature12477 (2013).
808	9	Petljak, M. & Alexandrov, L. B. Understanding mutagenesis through delineation of
809	-	mutational signatures in human cancer. Carcinogenesis 37, 531-540,
810		doi:10.1093/carcin/bgw055 (2016).
811	10	Pich, O. et al. The mutational footprints of cancer therapies. Nat Genet 51, 1732-1740,
812		doi:10.1038/s41588-019-0525-5 (2019).
813	11	Alexandrov, L. B. et al. The repertoire of mutational signatures in human cancer. Nature
814		<b>578</b> , 94-101, doi:10.1038/s41586-020-1943-3 (2020).
815	12	Alexandrov, L. B. et al. Clock-like mutational processes in human somatic cells. Nat
816		Genet 47, 1402-1407, doi:10.1038/ng.3441 (2015).
817	13	Alexandrov, L. B., Nik-Zainal, S., Siu, H. C., Leung, S. Y. & Stratton, M. R. A
818		mutational signature in gastric cancer suggests therapeutic strategies. Nat Commun 6,
819		8683, doi:10.1038/ncomms9683 (2015).
820	14	Alexandrov, L. B. et al. Mutational signatures associated with tobacco smoking in human
821		cancer. Science 354, 618-622, doi:10.1126/science.aag0299 (2016).
822	15	Fischer, A., Illingworth, C. J., Campbell, P. J. & Mustonen, V. EMu: probabilistic
823		inference of mutational processes and their localization in the cancer genome. Genome
824		<i>Biol</i> 14, R39, doi:10.1186/gb-2013-14-4-r39 (2013).
825	16	Mayakonda, A., Lin, D. C., Assenov, Y., Plass, C. & Koeffler, H. P. Maftools: efficient
826		and comprehensive analysis of somatic variants in cancer. Genome Res 28, 1747-1756,
827		doi:10.1101/gr.239244.118 (2018).
828	17	Blokzijl, F., Janssen, R., van Boxtel, R. & Cuppen, E. MutationalPatterns: comprehensive
829		genome-wide analysis of mutational processes. Genome Med 10, 33,
830		doi:10.1186/s13073-018-0539-0 (2018).

831 18 Ardin, M. et al. MutSpec: a Galaxy toolbox for streamlined analyses of somatic mutation 832 spectra in human and mouse cancer genomes. BMC Bioinformatics 17, 170, 833 doi:10.1186/s12859-016-1011-z (2016). 834 19 Gori, K. & Baez-Ortega, A. sigfit: flexible Bayesian inference of mutational signatures. 835 bioRxiv, 372896, doi:10.1101/372896 (2020). 836 20 Wang, S. et al. Copy number signature analyses in prostate cancer reveal distinct 837 etiologies and clinical outcomes. medRxiv, 2020.2004.2027.20082404, 838 doi:10.1101/2020.04.27.20082404 (2020). 839 21 Kasar, S. et al. Whole-genome sequencing reveals activation-induced cytidine deaminase 840 signatures during indolent chronic lymphocytic leukaemia evolution. Nat Commun 6, 841 8866, doi:10.1038/ncomms9866 (2015). 842 22 Taylor-Weiner, A. et al. Scaling computational genomics to millions of individuals with 843 GPUs. Genome Biol 20, 228, doi:10.1186/s13059-019-1836-7 (2019). 844 23 Degasperi, A. et al. A practical framework and online tool for mutational signature 845 analyses show inter-tissue variation and driver dependencies. Nat Cancer 1, 249-263, 846 doi:10.1038/s43018-020-0027-5 (2020). 847 24 Rosales, R. A., Drummond, R. D., Valieris, R., Dias-Neto, E. & da Silva, I. T. signeR: an 848 empirical Bayesian approach to mutational signature discovery. Bioinformatics 33, 8-16, 849 doi:10.1093/bioinformatics/btw572 (2017). 850 25 Gehring, J. S., Fischer, B., Lawrence, M. & Huber, W. SomaticSignatures: inferring 851 mutational signatures from single-nucleotide variants. *Bioinformatics* **31**, 3673-3675, 852 doi:10.1093/bioinformatics/btv408 (2015). 853 Consortium, I. T. P.-C. A. o. W. G. Pan-cancer analysis of whole genomes. *Nature* 578, 26 854 82-93, doi:10.1038/s41586-020-1969-6 (2020). 855 Kullback, S. & Leibler, R. A. On Information and Sufficiency. Ann. Math. Statist. 22, 79-27 856 86. doi:10.1214/aoms/1177729694 (1951). 857 Kuhn, H. W. The Hungarian method for the assignment problem. Naval Research 28 858 Logistics Quarterly 2, 83-97, doi:10.1002/nav.3800020109 (1955). 859 29 Huang, K., Sidiropoulos, N. D. & Swami, A. Non-Negative Matrix Factorization 860 Revisited: Uniqueness and Algorithm for Symmetric Decomposition. IEEE Transactions 861 on Signal Processing 62, 211-224, doi:10.1109/TSP.2013.2285514 (2014). 862 30 Lin, C. On the Convergence of Multiplicative Update Algorithms for Nonnegative Matrix 863 Factorization. IEEE Transactions on Neural Networks 18, 1589-1596, 864 doi:10.1109/TNN.2007.895831 (2007). 865 31 Bergstrom, E. N., Barnes, M., Martincorena, I. & Alexandrov, L. B. Generating realistic 866 null hypothesis of cancer mutational landscapes using SigProfilerSimulator. BMC 867 *Bioinformatics* **21**, 438, doi:10.1186/s12859-020-03772-3 (2020). 868 32 Tan, V. Y. F. & Févotte, C. Automatic Relevance Determination in Nonnegative Matrix 869 Factorization with the /spl beta/-Divergence. IEEE Transactions on Pattern Analysis and 870 Machine Intelligence 35, 1592-1605, doi:10.1109/TPAMI.2012.240 (2013). 871 33 Lawson, A. R. J. et al. Extensive heterogeneity in somatic mutation and selection in the 872 human bladder. Science 370, 75-82, doi:10.1126/science.aba8347 (2020). 873 34 Moody, S. et al. Mutational signatures in esophageal squamous cell carcinoma from eight 874 countries of varying incidence. bioRxiv, 372XXX (2020). 875 35 Gaujoux, R. & Seoighe, C. A flexible R package for nonnegative matrix factorization. 876 BMC Bioinformatics 11, 367, doi:10.1186/1471-2105-11-367 (2010).

877	36	Carpenter, B. et al. Stan: A Probabilistic Programming Language. Journal of Statistical
878		<i>Software</i> <b>76</b> , doi:10.18637/jss.v076.i01 (2017).
879	37	Schwarz, G. Estimating the Dimension of a Model. The Annals of Statistics 6, 461-464,
880		doi:10.1214/aos/1176344136 (1978).
881	38	Thorndike, R. L. Who belongs in the family? <i>Psychometrika</i> 18, 267-276,
882		doi:10.1007/bf02289263 (1953).
883	39	Benjamin, N., Raviteja, V., Miguel, A. HH., Svetlana, K. & Boian, A. A neural network
884		for determination of latent dimensionality in Nonnegative Matrix Factorization. Machine
885		Learning: Science and Technology (2020).
886	40	Kim, J. et al. Somatic ERCC2 mutations are associated with a distinct genomic signature
887		in urothelial tumors. Nat Genet 48, 600-606, doi:10.1038/ng.3557 (2016).
888	41	Cancer Genome Atlas Research, N. Comprehensive molecular characterization of
889		urothelial bladder carcinoma. <i>Nature</i> <b>507</b> , 315-322, doi:10.1038/nature12965 (2014).
890	42	Shalabi, L. A. & Shaaban, Z. in 2006 International Conference on Dependability of
891		Computer Systems. 207-214.
892	43	Žitnik, M. & Zupan, B. Nimfa: A python library for nonnegative matrix factorization.
893		The Journal of Machine Learning Research 13, 849-853 (2012).
894	44	Lew, J. et al. in 2019 IEEE International Symposium on Performance Analysis of Systems
895		and Software (ISPASS). 151-152.
896	45	Aranganayagi, S. & Thangavel, K. in International Conference on Computational
897		Intelligence and Multimedia Applications (ICCIMA 2007). 13-17 (IEEE).
898	46	Franc, V., Hlaváč, V. & Navara, M. in Computer Analysis of Images and Patterns. (eds
899		André Gagalowicz & Wilfried Philips) 407-414 (Springer Berlin Heidelberg).
900	47	Stacklies, W., Redestig, H., Scholz, M., Walther, D. & Selbig, J. pcaMethodsa
901		bioconductor package providing PCA methods for incomplete data. <i>Bioinformatics</i> 23,
902		1164-1167, doi:10.1093/bioinformatics/btm069 (2007).
903		

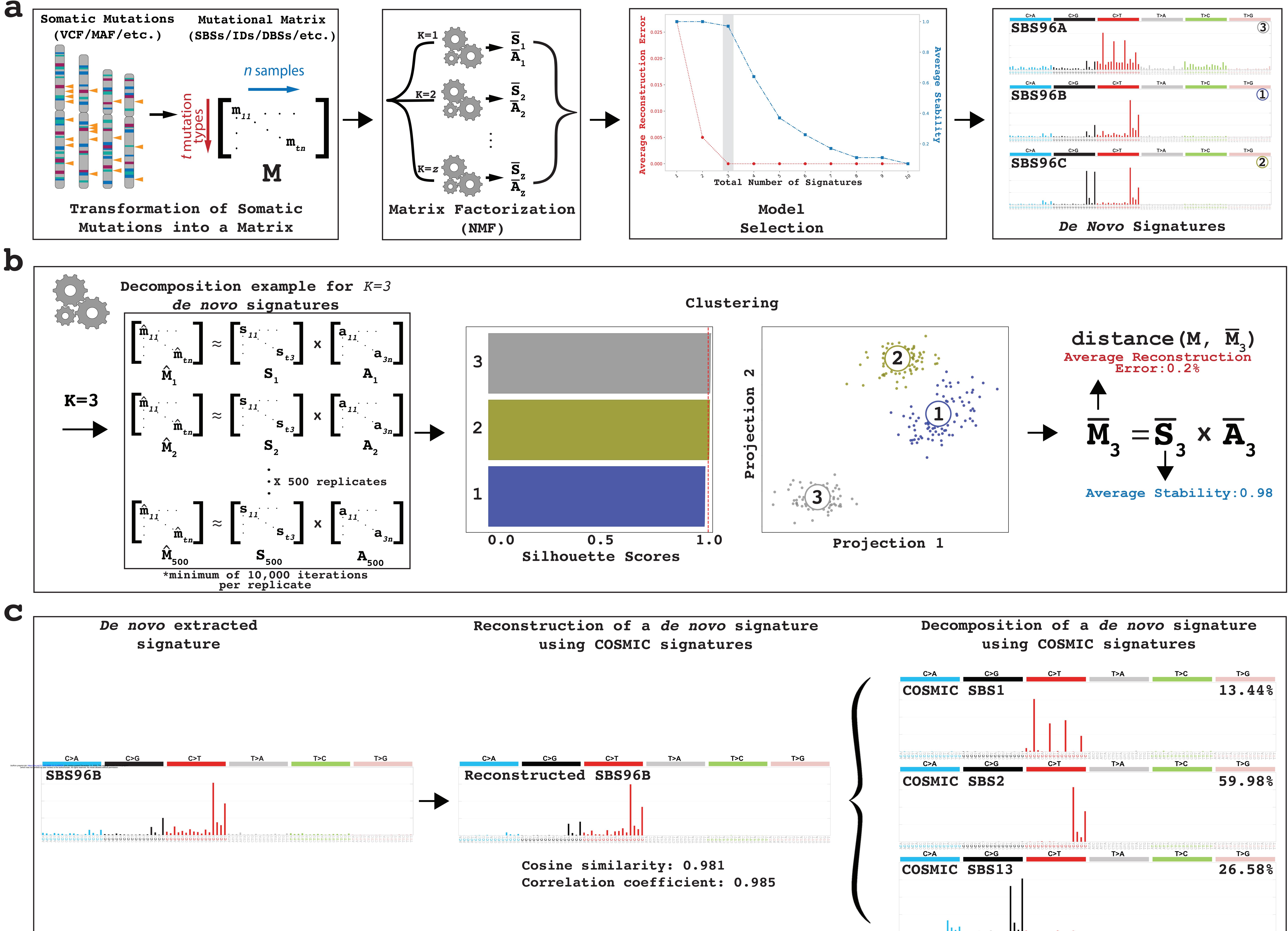
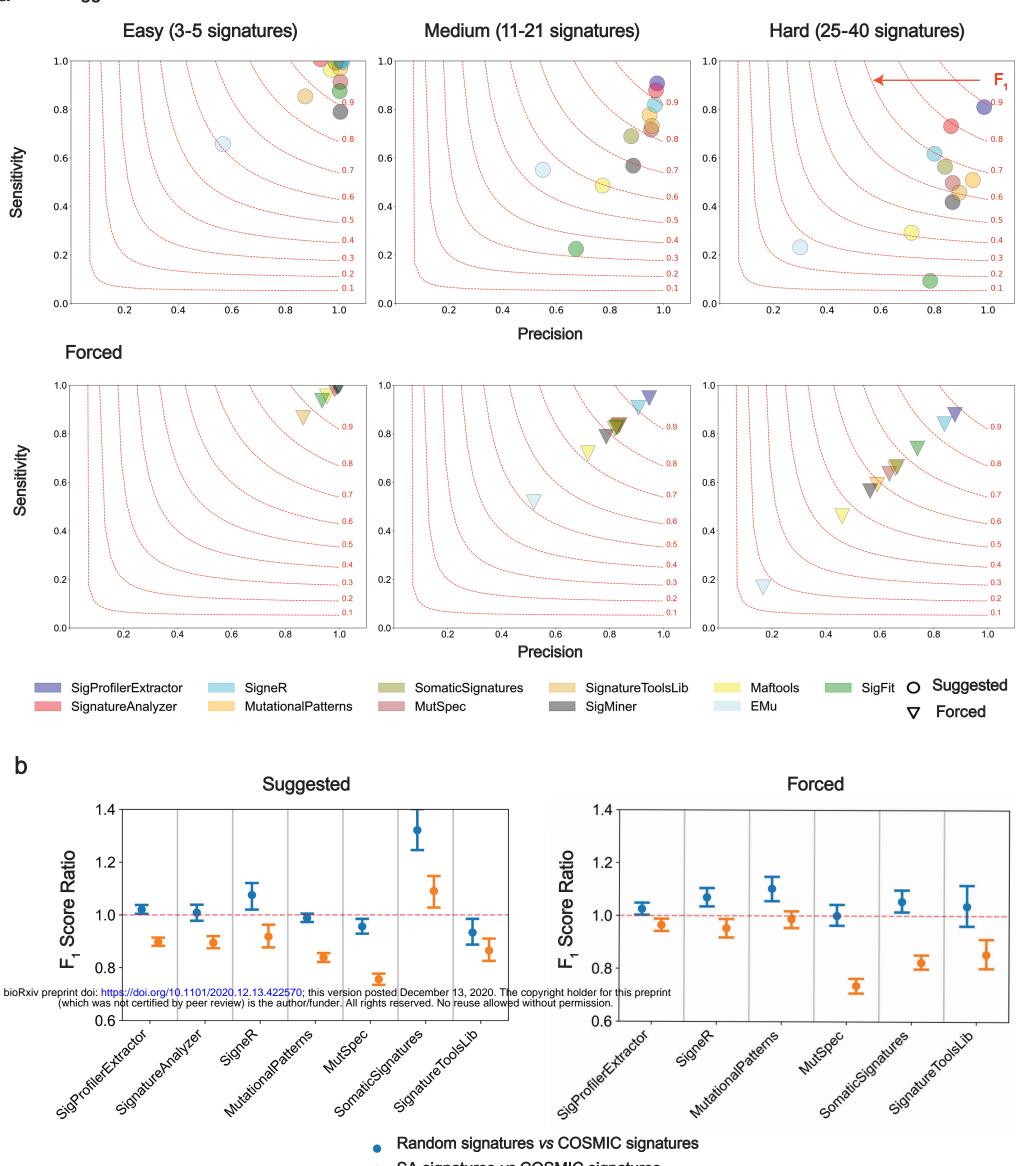


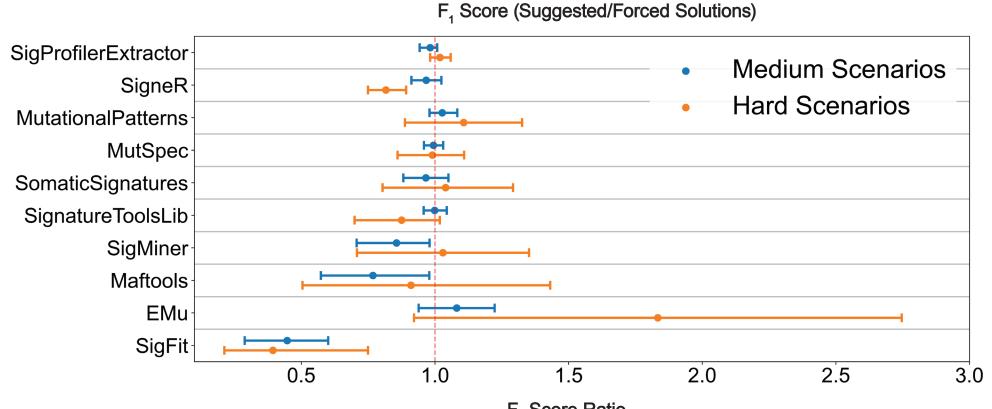
# Fig.2

С

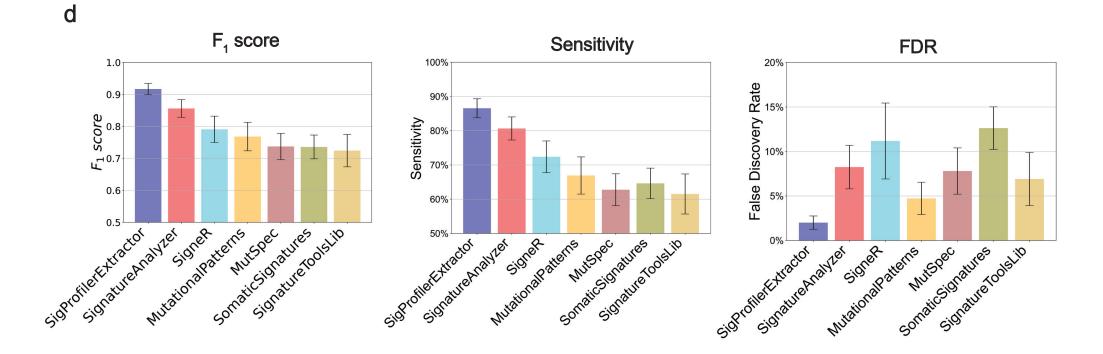
Suggested a

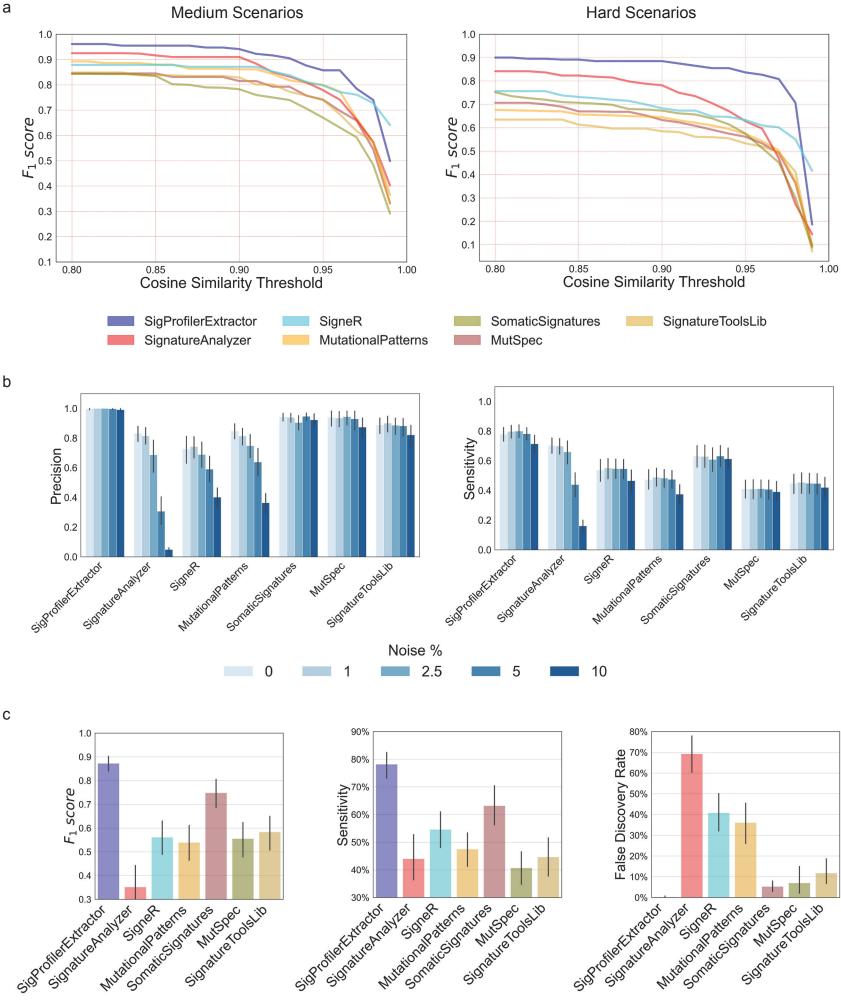


- Random signatures vs COSMIC signatures
- SA signatures vs COSMIC signatures



F<sub>1</sub> Score Ratio





а

